Journal of Hazardous Materials, 16 (1987) 267–292
Elsevier Science Publishers B.V., Amsterdam — Printed in The Netherlands

FEM3 MODEL SIMULATIONS OF SELECTED THORNEY ISLAND PHASE I TRIALS

S.T. CHAN, D.L. ERMAK and L.K. MORRIS

University of California, Lawrence Livermore National Laboratory, P.O. Box 808, Livermore, CA 94550 (U.S.A.)

(Received November 24, 1986; accepted February 20, 1987)

Summary

FEM3 is a three-dimensional computer model that was designed for simulating the atmospheric dispersion of heavy gas releases. The model, which has been actively used to simulate both continuous and finite-duration releases, is herein applied to and assessed for instantaneous heavy gas releases. The assessment is performed using some Thorney Island Phase I trials data. The selected trials, Nos. 9, 13, and 17, represent releases ranging from low wind speed and stable atmospheric conditions to strong wind and neutral stability, with initial relative density varying from 1.6 to 4.2. In this paper, a description of the model is given and model-data comparisons are made for the selected trials. Due to the inappropriateness of the present K-theory turbulence submodel for simulating the early phases of an instantaneous release, FEM3 consistently underpredicted the peak values of concentrations, sometimes by as much as a factor of 2. The shapes of the predicted peak concentration curves, however, agree favorably with field data. Overall, the FEM3 model appears to predict well most of the salient features present in large, instantaneous releases; specifically, gravity slumping and spreading, formation of the doughnut-shaped cloud, and cloud bifurcation. The predicted major cloud characteristics, including cloud area increase rates, critical distances and cloud arrival times, also agree well with field measurements.

1. Introduction

FEM3 is a three-dimensional computer model that was designed to simulate the atmospheric dispersion of large heavier-than-air gas releases [1]. The model employs a modified Galerkin finite element method [2] to solve the time-dependent conservation equations of mass, momentum, energy, and species, together with the ideal gas law for the density of the gas/air mixture. Turbulence is treated by using a K-theory submodel. These equations, along with submodels for the source and ground heat transfer, provide a mathematical description of the physics of heavy gas dispersion including gravity spread, the effect of density stratification on turbulent mixing, and ground heating into the gas cloud. Since it is fully three-dimensional, FEM3 can also treat complex flow and dispersion scenarios over variable terrain and around obstructions such as buildings.

0304-3894/87/$03.50

Over the past six years, the FEM3 model has been validated using a wide range of data obtained from both laboratory-scale and field-scale heavy gas dispersion experiments (discussed later in Section 2.1). These validation studies have not only greatly enhanced our knowledge in understanding the physics involved in heavy gas dispersion, but also provided us with the information necessary for model improvements. All the studies conducted so far, however, have been concerned with either finite-duration or continuous gas releases.

Recently an experimental program involving the instantaneous releases of large quantity of heavy gas was undertaken by the British Health and Safety Executive (HSE). The project, called the Heavy Gas Dispersion Trials, was organized by HSE as a cooperatively funded project with a total of 38 other organizations and the experiments were performed between 1982 and 1984 at Thorney Island, U.K. The field tests were divided into two phases and involved the instantaneous releases of about 2000 m^3 of a mixture of Freon-12 and nitrogen at ambient temperature, with mixture densities varying between 1.0 and 4.2 times that of air. In Phase I the dispersion was over uniform, unobstructed ground and comprised a total of 16 trials [3]. In Phase II, the dispersion took place in the presence of obstacles and comprised a total of 10 trials [4].

Compared to other field-scale experiments, the Thorney Island trials are unique in the following ways: (i) they are "instantaneous" releases involving a large amount of heavy gas, with density ratio as high as 4.2, and (ii) the containment structure (14 m in diameter and 13 m in height) alters profoundly the ambient wind field around the source and introduces significant wake effects. As a result, the flow field and the ensuing dispersion of the gas cloud are very complicated, especially during the early phases of the release. The purpose of this paper is to evaluate the performance of FEM3 in modeling the atmospheric dispersion of such large instantaneous releases using the data from a selected subset of Thorney Island Phase I trials.

2. The FEM3 model

2.1. Model development – Applications

The design of the FEM3 model was initiated in 1979 with the primary goal of developing a validated computer model for simulating the gravitational spread and vapor dispersion that result from an accidental spill of liquefied natural gas (LNG). Over the years, the model has been improved and generalized to treat also other heavier-than-air gases involving toxic and/or hazardous materials. An early version of FEM3, applied to simulate several of the Burro series LNG spill experiments [5], yielded results that correlated quite well with the field data [6]. In particular, the model successfully predicted the bifurcated structure of the vapor cloud in the Burro 8 test, which was conducted under low windspeed and stable atmospheric conditions. Since then,

FEM3 has been extended to treat variable terrain and the K-theory turbulence submodel has been improved to account for density stratification and ground heat transfer effects [7]. The study by Chan et al. [7] demonstrated that, under low windspeed and stable atmospheric conditions, even a relatively gentle terrain can greatly alter the size and shape of the hazardous area of a heavy gas cloud. The study also provided explanations of the formation of a bifurcated vapor cloud (in the form of horizontal cloud splitting and the vertically, nose-shaped cloud edges), due to various outward moving vortices induced by horizontal density gradients. A detailed assessment of the FEM3 model using the data obtained from both the Burro and the Coyote series of LNG spill experiments [5, 8] can be found in Morgan et al. [9].

Recently, a study utilizing the FEM3 model was conducted primarily to address the heavy gas effects [10], using the data from several field experiments [5, 11]. This study demonstrated that the presence of a heavier-than-air gas has two major effects: (i) reduction of turbulent mixing within the vapor cloud due to the stable stratification of the cloud layer, and (ii) generation of gravity spreading and vortices due to the presence of horizontal density gradients. These effects are competing in that the former tends to increase concentation levels by decreasing turbulent diffusion and the latter tends to decrease the concentration by entraining air through the top surface and the edges of the vapor cloud. The outcome of the combined effects depends mainly on the atmospheric and spill conditions. Specifically, for spills conducted under unstable atmospheric conditions and low spill rates, the reduction of turbulent mixing appears to be more important, resulting in slightly higher concentrations than a release of the same quantity of neutrally-buoyant material. On the other hand, for spills conducted under stable atmospheric conditions and high spill rates, the gravity spreading effects are usually more important, resulting in a much wider cloud with lower concentrations and a shorter downwind distance to the hazardous level.

More recently, FEM3 was applied [12] to simulate four of the refrigerated liquid propane spill tests conducted by Shell Research Limited [13]. In general, good agreement between model predictions and field data was observed. However, in the case of Spill 54, where an extremely low vapor cloud was produced and heavy gas effects were more dominant, the existing turbulence submodel was observed to perform less satisfactorily, thus prompting the development of an improved turbulence submodel [14]. This submodel was developed utilizing the detailed experimental data obtained by McQuaid [15] in his wind tunnel investigation of the structure of shear flows with stable density stratification.

Other capabilities and applications of the FEM3 model include a simple submodel for treating aerosol effects in the pressurized ammonia (NH_3) spills [16], a phase-change submodel to treat humidity in the ambient atmosphere

[17], and the use of FEM3 as a tool for emergency-response planning for potential accidental releases of liquid chlorine [18].

2.2 Governing equations

A detailed description of the FEM3 model is given by Chan [1] and the numerical method of solution is described by Gresho et al. [2]. The FEM3 model solves the following three-dimensional, time-dependent conservation equations:

$$\frac{\partial(\rho\mathbf{u})}{\partial t}+\rho\mathbf{u}\cdot\nabla\mathbf{u}=-\nabla p+\nabla\cdot(\rho\mathbf{K}^{\mathrm{m}}\cdot\nabla\mathbf{u})+(\rho-\rho_{\mathrm{h}})\mathbf{g}, \tag{1}$$

$$\nabla\cdot(\rho\mathbf{u})=0, \tag{2}$$

$$\frac{\partial\theta}{\partial t}+\mathbf{u}\cdot\nabla\theta=\frac{1}{\rho C_{\mathrm{P}}}\nabla\cdot(\rho C_{\mathrm{P}}\mathbf{K}^{\theta}\cdot\nabla\theta)+\frac{C_{\mathrm{PN}}-C_{\mathrm{PA}}}{C_{\mathrm{P}}}(\mathbf{K}^{\omega}\cdot\nabla\omega)\cdot\nabla\theta, \tag{3}$$

$$\frac{\partial\omega}{\partial t}+\mathbf{u}\cdot\nabla\omega=\frac{1}{\rho}\nabla\cdot(\rho\mathbf{K}^{\omega}\cdot\nabla\omega), \tag{4}$$

and

$$\rho=\frac{PM}{RT}=\frac{P}{RT\left(\dfrac{\omega}{M_{\mathrm{N}}}+\dfrac{1-\omega}{M_{\mathrm{A}}}\right)}, \tag{5}$$

where $\mathbf{u}=(u, v, w)$ is the velocity, ρ is the density of the mixture, p is the pressure deviation from an isothermal atmosphere at rest with corresponding density ρ_{h}, $\mathbf{g}$ is the acceleration due to gravity, θ is the potential temperature deviation from an adiabatic atmosphere at θ_0, ω is the mass fraction of the dispersed species, $\mathbf{K}^{\mathrm{m}}$, $\mathbf{K}^{\theta}$, and $\mathbf{K}^{\omega}$ are the eddy diffusion tensors for momentum, energy, and the dispersed species, and C_{PN}, C_{PA}, and $C_{\mathrm{p}}=\omega C_{\mathrm{PN}}+(1-\omega)C_{\mathrm{PA}}$ are the specific heats for the species, air, and the mixture, respectively. In the equation of state, P is the absolute pressure, R is the universal gas constant, M_{N}, M_{A} are the molecular weights of the species and air, and T is the absolute temperature ($T/(\theta+\theta_0)=(P/P_0)^{R/MC_{\mathrm{p}}}$). For problems of current interest, because the heights of interest are generally small ($\ll 1$ km), the ratio P/P_0 is approximately equal to unity and hence no distinction is made between the absolute and potential temperature in the present model (which is fortunate since the last equation is strictly valid only when M is constant). The above set of equations, together with appropriate initial and boundary conditions, are solved to yield the mean values of velocity, pressure, temperature, mass fraction of the dispersed species, and density of the mixture as functions of time and space.

The above set of equations were obtained by generalizing the anelastic approximation of Ogura and Phillips [19]. The essential features of the present (generalized anelastic) conservation equations are that variable density is allowed and yet sound waves are filtered a priori (thus time steps are not restricted by acoustic effects). The proper interpretation of neglecting $\partial\rho/\partial t$ in eqn. (2) for mass conservation is that acoustic density variations in time are of very small amplitude and occur so quickly that it is a good approximation to assume density is always in equilibrium with the other thermodynamic variables. The time dependence of density is then determined implicitly by the time variation of temperature, pressure, and composition via the ideal gas law. It is not appropriate to interpret eqn. (2) as implying $\partial\rho/\partial t=0$, since ρ does indeed vary with time. More detailed discussions of the generalized anelastic formulation can be found in Lee et al. [20]. It is to be noted that the turbulence diffusion terms in eqns. (3) and (4) differ slightly from those given in Ref. [20]. The current form is more appropriate when the spatial variations of density and specific heat are significant.

2.3 Turbulence submodel

FEM3 treats turbulence by using a K-theory local equilibrium model. The turbulent diffusion tensors $\mathbf{K}^{m}$, $\mathbf{K}^{\theta}$, and $\mathbf{K}^{\omega}$ are assumed to be diagonal and it is further assumed that $\mathbf{K}^{\theta}=\mathbf{K}^{\omega}$. Specifically, the vertical diffusion coefficient is given by

$$K_V=\frac{k[(u_* z)^2+(w_* h)^2]^{1/2}}{\Phi} \tag{6}$$

where k = von Karman's constant, 0.4; u_* = friction velocity, $u_{a*}\cdot|u/u_a|$ in which u is the windspeed and subscript "a" designates the ambient atmosphere; z = height above ground surface; w_* = in-cloud "convection velocity", $\alpha_1[(g/T)v_E(T_{gr}-T)h]^{1/3}$; α_1 = empirical constant for in-cloud convection, 0.5; h = cloud height function, $\bar{z}\cdot\exp(1-z/\bar{z})$; $\bar{z}$ = characteristic cloud height, $\int\omega z\,dz/\int\omega dz$; g = acceleration of gravity; T = cloud temperature; T_{gr} = ambient ground temperature; v_E = effective heat-transfer velocity from the ground into the vapor cloud; and Φ = Monin–Obukhov profile function.

The form of the Monin–Obukhov profile function Φ is taken from Dyer [21]. When the Richardson number (Ri, to be defined later) is greater or equal to zero, Φ is defined as

$$\Phi=1+5Ri, \qquad Ri\geq 0 \tag{7a}$$

for all three (momentum, energy, and species) vertical diffusion coefficients. When the Richardson number is less than zero, Φ is defined as

$$\Phi = \begin{cases} (1-16\mathrm{Ri})^{-1/4} \text{ for momentum,} \\ (1-16\mathrm{Ri})^{-1/2} \text{ for energy and species.} \end{cases} \qquad \mathrm{Ri}<0 \qquad (7b)$$

The above equation indicates that, as the Richardson number becomes increasingly negative, the effects of convection are felt more strongly on the turbulent transport of heat and species than on momentum.

The local Richardson number is, in turn, defined by an *ad hoc* approach to be

$$Ri = u_*^2 \frac{Ri_a}{(u_*^2+w_*^2)} + \alpha \frac{(\rho-\rho_a)}{\rho} \frac{gh}{(u_*^2+w_*^2)} \qquad (8)$$

where Ri_a and ρ_a are the Richardson number and density of the ambient atmosphere ($Ri_a = z/L$, L being the Monin–Obukhov length scale for the ambient atmosphere), and α is an empirical parameter for the density stratification effect, currently taken to be 0.05.

The horizontal diffusion coefficient, K_h, is expressed as

$$K_h = \beta k u_* z/\Phi \qquad (9)$$

where $\Phi = \Phi(Ri_a)$ and β is an empirical parameter with a value of 6.5, which was inferred from the Pasquill–Gifford curves for the horizontal and vertical dispersion coefficients σ_y and σ_z.

The first term on the right hand side of eqn. (8) is designed to include the turbulence in the ambient atmosphere and the second term represents the effects of density stratification which is generally a reduction of turbulence in the stably stratified, dense gas cloud. As can be seen, for isothermal, neutrally buoyant gas or in the absence of a dispersing cloud, the present submodel recovers the ambient diffusivities.

Under neutral ambient conditions ($Ri_a = 0$) with no ground heating ($u_* = 0$), the above Richardson number (due to density stratification) becomes

$$Ri_d = \alpha \frac{(\rho-\rho_a)gh}{\rho u_*^2} \qquad (10)$$

where $u_* = |u/u_a|\, u_{a*}$, and $h = \bar{z} \exp(1-z/\bar{z})$.

Examination of the variation of Richardson number with height assuming typical vertical density profile shows two major deficiencies in the above model:

(i) The evaluation of the friction velocity u_* using a scaling factor of the ratio of the resulting flow speed and the ambient windspeed is inappropriate in the source region. Here, the flow velocities are usually very low so that u_* approaches zero and unreasonably large values of the Richardson number are generated.

(ii) The vertical profile of the Richardson number has a maximum value at the ground surface and monotonically decreases to the ambient value (zero for neutral ambient conditions). Such a shape is inconsistent with the more physically-motivated idea that suggests a zero value at ground level and a maximum value near the top of the cloud where the density gradient is largest.

As remedies to the above deficiencies, two alternative submodels were investigated by Ermak and Chan [14] and the following formula for defining density stratification effects on the Richardson number was selected for further testing and evaluation. Using the concept of the gradient Richardson number

$$Ri = -\frac{g\,(\partial\rho/\partial z)}{\rho(\partial u/\partial z)^2}$$

and the following assumptions:

$$\rho - \rho_a = (\rho - \rho_a)_{z=0} \cdot exp[-(z/h_c)^n]$$

and

$$u = \frac{u_*}{k} ln(z/z_0)$$

the following Richardson number is obtained to replace eqn. (10)

$$Ri_d = nk^2(z/h_c)^n \cdot \frac{(\rho - \rho_a)gz}{\rho u_*^2} \tag{11}$$

In the calculations to be presented herein, the exponent n is taken to be 2, based on McQuaid's measured concentration profiles [15].

For the friction velocity, since the simple scaling by windspeeds was found unsatisfactory in the source region [14], a zeroth order approximation is currently used, i.e., $u_* = u_{a*}$. This approximation eliminates the possibility of u_* approaching zero near the source and also gives the correct value of friction velocity as the flow approaches the ambient condition. While it provides a good approximation for a large part of the flow, a more reliable estimate is obviously needed for the regions where velocities are significantly perturbed, either by the presence of obstacles or a heavy gas cloud. Such an improvement is being investigated.

The characteristic cloud height is taken to be

$$h_c = \frac{1}{\omega_{max}} \cdot \int \omega dz$$

Typical Richardson number profiles obtained with eqns. (10) and (11) in the presence of a heavy gas cloud are shown in Fig. 1. As is seen, the present submodel has a zero value at ground level and a maximum value near the top

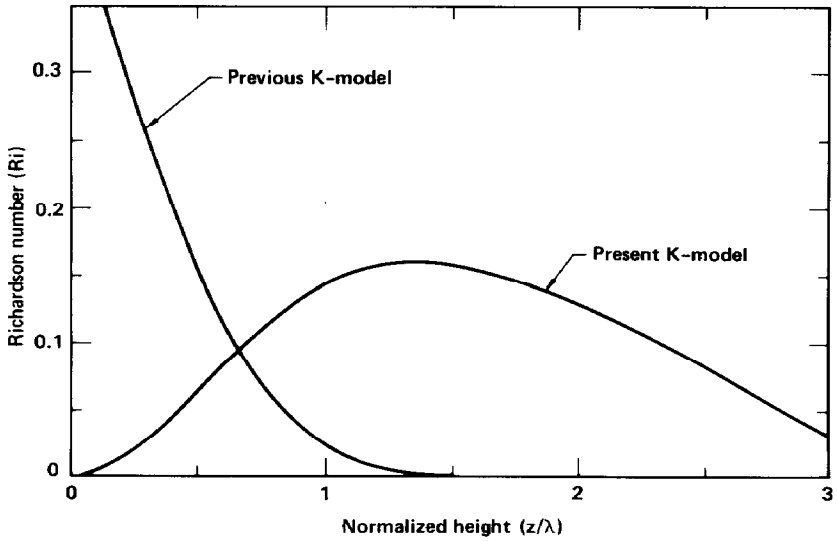

Fig. 1. Typical Richardson number profiles obtained from the present and previous K-models (λ being the height with 50% ground level concentration).

of the cloud where large density gradient and small shear stress exist. Results from this improved K-model were found to best match McQuaid's data (of laboratory-scale,continuous releases) with the Richardson number defined in eqn. (11) modified by a factor of 0.2. In McQuaid's experiments, because the concentration profile is Gaussian, it would be more realistic to take $h_c = (2/\omega_{max}) \int \omega \, dz$ and this factor of 2, with $n = 2$ in eqn. (11), would (almost) account for the factor of 0.2 found necessary for such cases. For the instantaneous releases reported herein, however, the use of such a factor was observed to yield insufficient turbulence damping and thus is not being used. These results suggest that the concentration profile is not Gaussian.

2.4 Source description

The source submodel described in Chan [1] and later refined in Chan and Ermak [12] was designed for spills involving either continuous or finite-duration gas releases. For the Thorney Island trials, an instantaneous source submodel is required. In the prsent FEM3 model, this is done by designating a block of mesh points (or blocks of mesh points for multiple sources) to represent the desired source structure filled with the material to be released. Appropriate initial concentration and, for non-isothermal releases, the temperature as well, are specified at these mesh points. In order to minimize the spatial oscillations in the concentration and temperature solutions due to the presence of short wave lengths (relative to the grid spacings) in the initial conditions (typically of the step-function-type), the initial concentration and

temperature fields are often extended (smoothed) by trivariate Gaussian functions in the region immediately surrounding the nodes representing the source structure. For the simulations presented herein, a cube of 12 meters on each side was selected to represent the source, within which the initial velocity was set to be zero and a constant concentration value (based on the given initial relative density) was specified. The amount of source material within the cube plus the trivariate Gaussian functions with a standard deviation of 1 m gave approximately the desired amount of gas mixture in each case. The decision to use a cube, rather than the form of a near cylinder (a twelve-sided polygon actually) 14 m across and 13 m high, to represent the source structure was based on considerations of reducing computing costs. The effects resulting from such a discrepancy in representing the source are likely to be secondary, compared to other uncertainties such as turbulence parameterization and the sparseness of field measurements available for comparisons.

3. Model–data comparisons

3.1 Summary of selected trials

Three of the Thorney Island Phase I trials, Nos. 9, 13, and 17, have been selected for this study. The atmospheric and release conditions for these trials, based on the data given by Davies and Singh [22] and McQuaid [3], are summarized in Table 1. Trial No. 9 represents releases under low windspeed and stable atmospheric conditions, Trial No. 13 is a release under strong wind and neutral stability, and Trial No. 17 has the highest initial relative density among all trials, together with moderate windspeed. The initial Richardson number in the table is defined as in [3]:

$$Ri_0 = g\frac{(\rho_0 - \rho_a)}{\rho_a}\frac{H_0}{U_{10}^2}$$

where ρ_0 and H_0 are the initial mixture density and cloud height, respectively. The Richardson number is a measure of the importance of the buoyancy force relative to the mechanical shear (or drag) of the ambient atmosphere. As can be seen, the buoyancy force is predominant initially in all cases except, perhaps, for Trial No.13.

The time series of HSE concentration data [23] and the analyzed data available in the open literature furnish the basis for the present model–data comparisons. Linear interpolation in the crosswind direction was applied to the peak values of the concentration and an adjacent value at the same time to provide data suitable for such comparisons. For brevity, only the results from Trial No. 9 (which has the highest initial Richardson number) will be presented and discussed in more detail relative to the other two cases.

TABLE 1

Atmospheric and release conditions for three selected Thorney Island trials

Trial number	9	13	17
Volume released (m^3)	2000	1950	1700
Initial relative density	1.60	2.00	4.20
Windspeed at 10 m (m/s)	1.7	7.5	5.0
Friction velocity (m/s)	0.10	0.40	0.28
Monin-Obukhov length scale (m)	15	−129	125
Surface roughness length (mm)	10	5	7
Pasquill stability category	F	D	D/E
Initial Richardson number	26.5	2.2	13.8

3.2 Trial No. 9

As indicated earlier, Trial No. 9 was conducted under low wind speed and stable atmospheric conditions; thus, gravity force is expected to play a much more important role than it does in the other two cases. For this trial, a graded mesh consisting of a total of 7,488 mesh points (13 vertically, 16 laterally, and 36 longitudinally) was used for the following computational domain: $x = -100$ to 400 m longitudinally, $y = 0$ to 160 m laterally, and $z = 0$ to 40 m vertically. The mean wind was assumed to be parallel with the center plane of the source, which is centered above the origin of the coordinate system. Due to symmetry of the gas cloud, only one-half of the cloud needs to be simulated. The velocity profile on the upwind boundary was based on the measured wind profile [22] and specified to be

$u = 0.40 + 0.23z - 0.01z^2$ m/s for $z < 11.5$ m

and

$u = 1.75$ m/s for $z \geqslant 11.5$ m.

Simulation of the gas dispersion was performed in two stages. Firstly, the flow field over and around the source was calculated for a sufficient period of time to obtain an approximately steady wind field with the velocity and pressure values at nodes corresponding to the source volume set to be zero. This is equivalent to solving for the steady state flow field around the containment structure. Secondly, the above constraints were removed (at $t = 0$) to simulate the instantaneous release of the source material. The released gas mixture was then subjected to the ensuing physical processes including gravity slumping and spreading, wake turbulence effects, density stratification, and the coupling between the gas cloud and the surrounding wind field.

Figures 2 and 3 show respectively several views of the steady state velocity field in the vicinity of the containment structure prior to the gas release. No attempt was made herein to resolve the very thin boundary layers ($\delta \ll 1$ m)

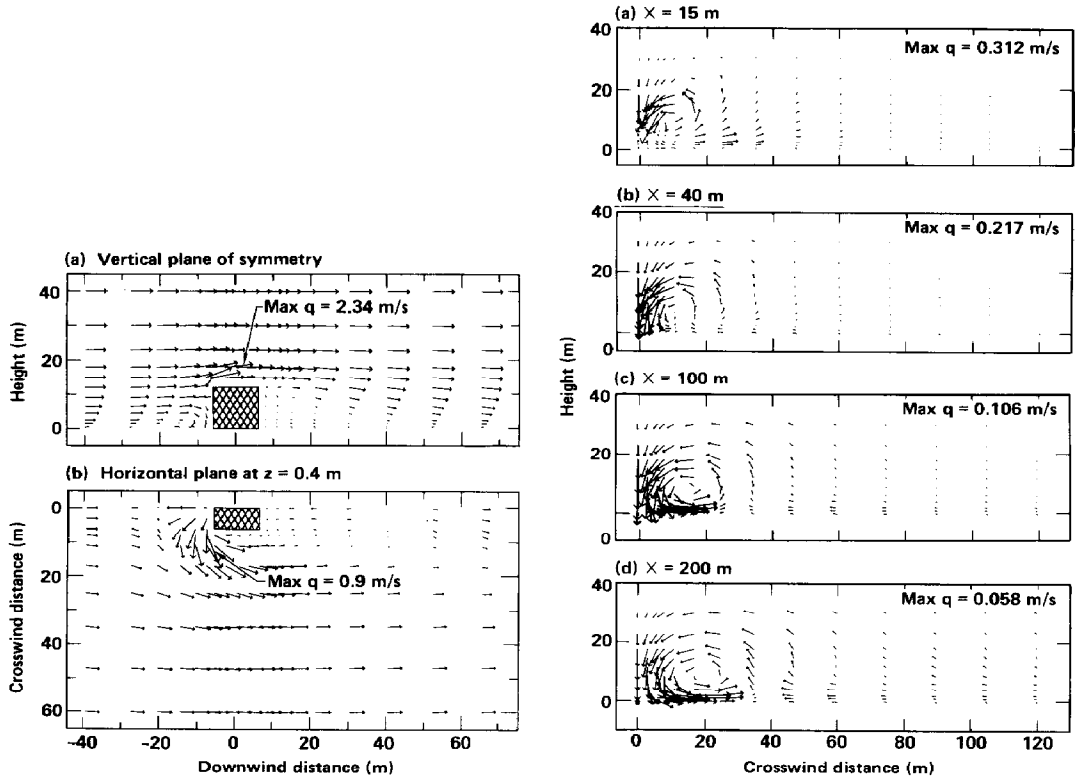

Fig. 2. Two views of the predicted velocity field around the source of Thorney Island Trial No. 9.

Fig. 3. Predicted velocities at various crosswind planes behind the source of Thorney Island Trial No. 9.

on the walls of the source structure, because the computational cost in doing so would have been prohibitively expensive. Additionally, such fine-scale features exist only prior to the gas release and thus their effects on the gas dispersion are likely to be limited to early times only, when gravity forces are dominating. For these reasons, the approach adopted here is to use a variable grid (1 m or so near the source and about 10 m in the far field) to capture the more important medium- and large-scale features of the flow field. Shown in Fig. 2(a) are the velocity vectors on the vertical symmetry plane. A recirculating region is created at the windward side of the source. Over the top surface, the flow accelerates and finally reattaches at about 50 m behind the source, thus creating a much larger recirculating region and low pressure in the leeward side of the source structure. Figure 2(b) is a horizontal view of the velocity projection at a height of 0.4 m (the height of the first node from ground level), where the air flow is seen to accelerate and move sideward, resulting in

low pressure regions on the sides (not shown here). Another feature of the flow field over the source obstruction is the generation of a pair of horseshoe-shaped trailing vortices, one of which is depicted in Fig. 3. In this figure, velocity projections on four crosswind planes at various downwind distances are shown. Notice the change in location and the decrease in intensity of the vortex along the downwind direction. These features of the flow field have been commonly observed in air flow around buildings and will obviously affect the subsequent gas dispersion. These effects, in the present case, may not be too strong due to the dominance of gravity during early times and the temporary nature of the source obstruction (in the experiments, the plastic curtain containing the source material was designed to drop completely in less than 2 s). However, for heavy gas dispersion over and around a permanent obstruction, the above effects could be very significant.

Figures 4 and 5 illustrate the evolution of the gas cloud and the associated velocity vectors on the vertical symmetry plane and the 0.4 m horizontal plane for the first 6 s after the release. During this initial slumping phase, the gravity force is clearly dominating and has created a nearly axisymmetric flow field (see Fig. 5). However, as shown in Fig. 4, both the velocity vectors and the concentration contours are not strictly symmetric about the centerline of the source on the vertical plane. In particular, the velocity vectors display more asymmetry, owing to the much-altered, ambient wind field caused by the source structure. The windward vortex is seen to be greatly enhanced while the leeward vortex in the wake is affected mostly near the ground only. As a result, the downward moving jet and the upper part of the vapor cloud have been shifted noticeably toward the downwind direction. The maximum wind speed on this plane has increased to 11.8 m/s at the end of 6 s and was observed to decrease afterward.

In Fig. 5, a plan view of the velocity vectors and concentration contours at a height of 0.4 m are shown. Gravity slumping has produced a nearly axisymmetric flow field and an almost concentric cloud shape near the ground. Because the source cube has a lower pressure along its sides than that on the rear surface, the gas cloud spreads slightly more in the lateral than the downwind direction. The contour plots on the right of Fig. 5 show how one-half of a nearly concentric ring of the gas cloud is formed at the end of 6 s. Such a physical process has been described and explained by Rottman et al. [24]. As the heavy gas cloud collapses, it spreads radially. The fluid in the cloud accelerates as it spreads radially except for the fluid near the current front. The front is inhibited from moving as fast as the following current of heavy fluid because it effectively experiences a "drag" caused by the inertia and shear stresses involved in accelerating the surrounding fluid. The net effect is that most of the heavy gas becomes concentrated in a narrow expanding ring. Despite some wiggles [25] in the concentration field at $t=6$ s, the above salient features of the velocity and concentration fields are well-reproduced.

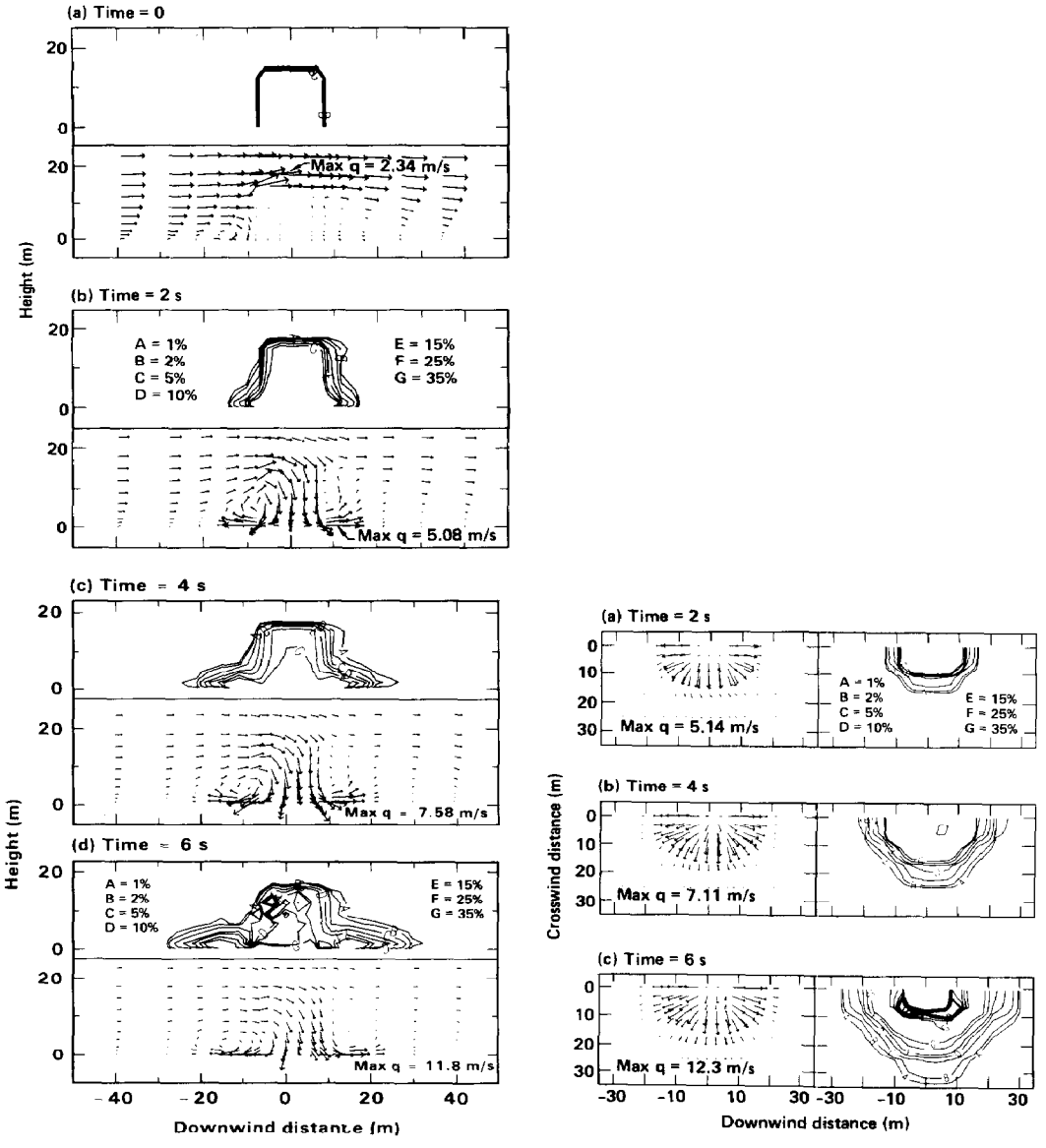

Fig. 4. Predicted concentration contours and velocities along the vertical plane of symmetry for Thorney Island Trial No. 9.

Fig. 5. Predicted velocity vectors and concentration contours for Thorney Island Trial No. 9 (at height = 0.4 m).

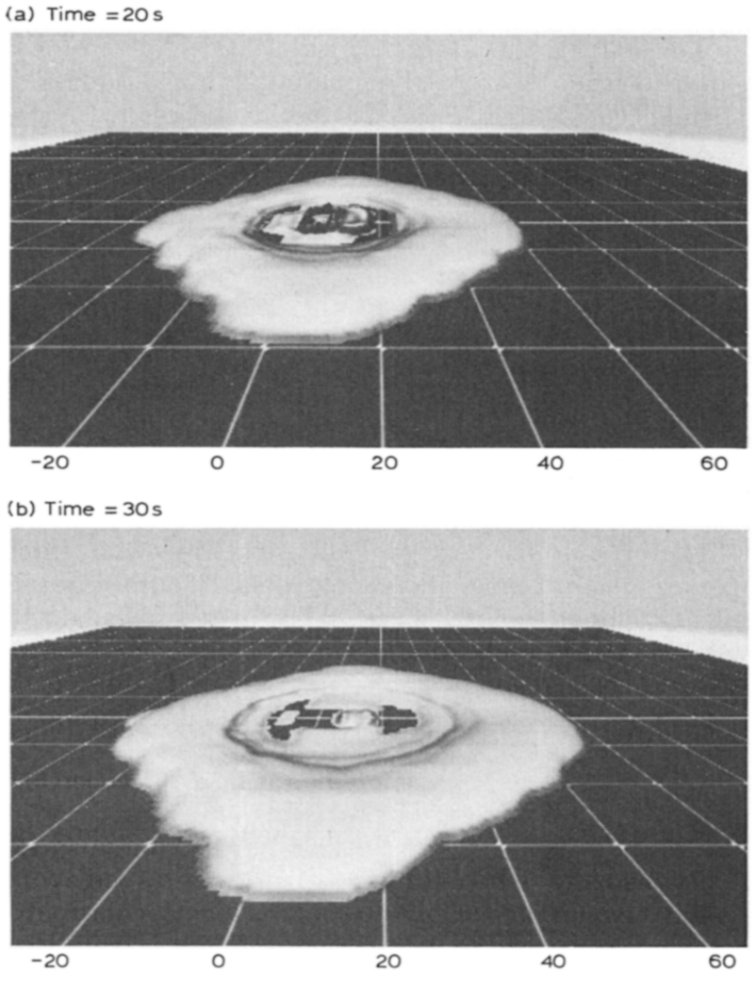

Fig. 6. Pictorial views of the 1% concentration cloud surfaces for Thorney Island Trial No. 9.

In Fig. 6, two computer-generated pictorial views of the 1% concentration cloud surfaces at $t = 20$ and 30 s are displayed. The viewer is positioned 180 m above the cloud, 130 m to the side and 20 m downwind from the source center, looking back towards the source. Because the viewer is close to the cloud, there is a visual distortion of the cloud on the viewer's side which is indicated by the equally-spaced grid underneath. The mean wind is blowing from left to right and the grid lines shown are 20 m apart (these are not the calculational grid lines). At $t = 20$ s, the cloud dimensions are approximately 120 m (-55 m to 65 m) in length, 120 m in width and about 5 m in height. Due to the presence of a pre-existing wind, the gas cloud has shifted slightly toward the downwind direction. Nevertheless, the gas cloud remains basically in a doughnut shape,

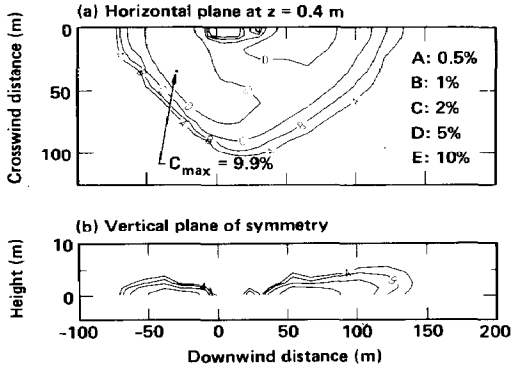

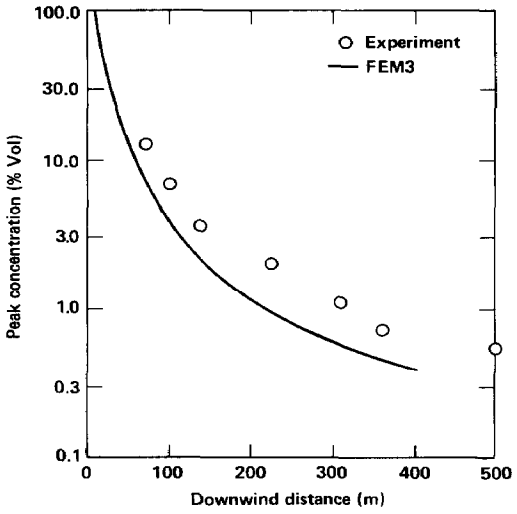

Fig. 7. Predicted concentration contours for Thorney Island Trial No. 9 at $t = 75$ s.

Fig. 8. Predicted versus measured peak concentrations for Thorney Island Trial No. 9 (at height = 0.4 m).

as observed in laboratory calm-wind releases (see, for example, Fig. 3 of Spicer and Havens [26]). By $t = 30$ s, the cloud has spread to about 140 m in both length and width, while its height decreased slightly. This gravity-spreading phase continues for about 60 more seconds before sufficient kinetic energy has been dissipated and the cloud ceases to expand. It has been brought to our attention by Dr. McQuaid that very extensive photographic records exist of the clouds, which could be very valuable in aiding our model assessment. Hopefully, some use can be made of such experimental records in our further analysis of the results.

In Fig. 7, the predicted concentrations at $t = 75$ s (in % volume of the original Freon-12/nitrogen mixture) on the 0.4 m horizontal plane and the vertical symmetry plane are shown. At this time, although the cloud has been diluted to about 10% in concentration, the width-to-length ratio of the gas cloud remains near unity, indicating that gravity spreading has been dominant up to this time. The 1% concentration contour in the simulation continued to expand to a maximum extent of 70 m upwind and to nearly 220 m in width. The maximum height of the 1% contour at this time was about 4 m and decreased slowly during the rest of the 420 s simulation. Of particular interest here are the cloud bifurcation (see the region enclosed by the 5% contour on the horizontal plane) and the highly diluted cloud center. While the former has been observed in large, continuous releases under stable conditions (see, for example, Chan et al. [7]), the latter is unique to instantaneous spills due to the initial gravity slumping.

In Fig. 8, the predicted peak values of concentration on the 0.4 m horizontal plane are compared with the measured peak concentrations on, or near, the path of the cloud centroid, as taken from McQuaid [3] and the HSE data reports [23]. Although the FEM3 predictions are consistently below the data by as much as a factor of two, the predicted shape of the curve shows very good agreement with the field measurements. The present discrepancies can be attributed to several factors. Firstly, the present K-theory submodel has not been designed and is not intended for simulating the initial phases of gravity slumping and spreading in instantaneous spills. The premises of the current turbulence submodel are local equilibrium and the similarity functions and velocity profiles that are based on measurements in steady atmospheric boundary layers with virtual homogeneity in the horizontal directions. In contrast, the release of an instantaneous heavy gas is generally highly transient with complex flow phenomena involving gravity slumping and the generation and transport of various scales of vortices. A more sophisticated turbulence submodel (such as transport equations) would be necessary to model the turbulence more accurately during such initial phases of an instantaneous spill. Secondly, the FEM3 predicted mean values are being compared with data obtained from one experimental realization. Ideally, the predictions from a numerical model such as FEM3 should be compared with results of an ensemble average, where the ensemble consists of repeated releases with the "same" spill and atmospheric conditions to help compensate for the variability of field experiments [27]. Thirdly, although a 0.6 s averaging time was considered to be appropriate for the Thorney Island trials, based on the criterion of suppressing sensor noise [28], it is not clear that this averaging time is also appropriate for model validation purposes with three-dimensional numerical models such as FEM3. It is difficult to define precisely the averaging time appropriate for the FEM3 model, as such a time scale is generally problem dependent. In theory, the appropriate averaging time should be such that it is much longer than that associated with turbulent quantities and yet is short enough for describing the characteristics of a transient gas cloud. Based on the wind speeds and grid spacings currently used, an averaging time of 1 to 2 s is probably more appropriate for the selected trials. Nussey et al. [28] stated that an averaging time of 3 s could reduce the peak concentration values based on a 0.6 s average by as much as a factor of 2, which would have generated better agreement between model predictions and field data. On the other hand, due to the wide spacing of the sensor array in the crosswind direction, the actual peak values in the experiment could be higher than those recorded, thus making the discrepancy even larger. These are difficult questions inherent in any field validation program.

3.3. Trial No. 13

Trial No. 13 was conducted under a high wind speed of 7.5 m/s and neutral atmospheric conditions. Under such conditions, a narrower and more rapidly

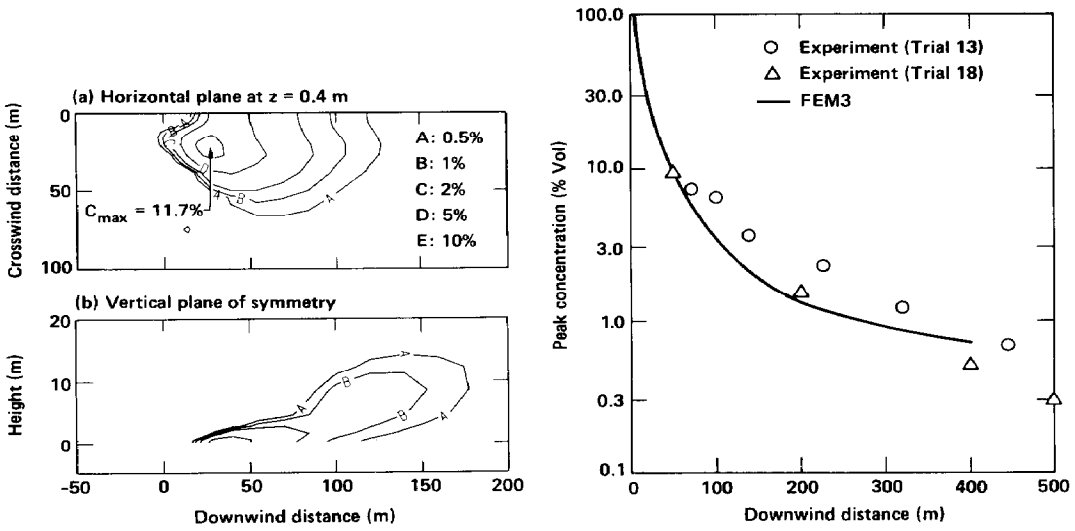

Fig. 9. Predicted concentration contours for Thorney Island Trial No.13 at $t=25$ s.

Fig. 10. Predicted versus measured peak concentrations for Thorney Island Trial Nos. 13 and 18 (at height = 0.4 m).

diluted gas cloud (compared to that of Trial No. 9) is expected, thus fewer mesh points are required. For this trial, a graded mesh of 4,320 mesh points (10 vertically, 12 laterally, and 36 longitudinally) was used. The computational domain was: $x-100$ to 400 m longitudinally, $y=0$ to 100 m laterally, and $z=0$ to 30 m vertically. Again,due to symmetry, only one-half of the gas cloud needs to be calculated. The upwind velocity profile was specified to be

$$u=5.5+0.24z-0.004z^2 \qquad m/s.$$

Unlike Trial No. 9, gravity slumping in this trial was observed to last for only about 2 s. This trial is characterized by a narrower, relatively high gas cloud, with much weaker cloud bifurcation (the lateral edges of the cloud are less elevated and the maximum concentration is closer to the cloud center line). The main mechanism for cloud bifurcation is the complex vortex system generated by the horizontal density gradients. In this trial, however, the higher values of windspeed and turbulence level have, in effect, weakened the vortex strength and produced a less bifurcated cloud. The maximum extent of the 1% concentration was only 20 m upwind and 130 m in the crosswind direction. Representative results from the gas dispersion simulation are presented in the following two figures. In Fig. 9, the predicted concentrations on the 0.4 m horizontal plane and the vertical symmetry plane are shown at the time when the cloud has been diluted to be near 10%. In Fig. 9(a), the upwind indentation of the cloud corresponds to the early, much-diluted source center and the down-

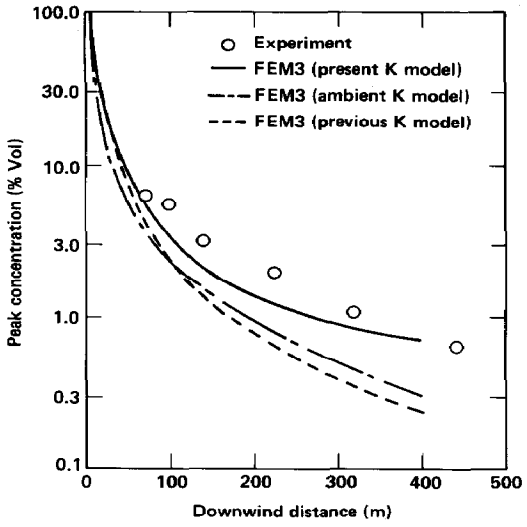

Fig. 11. Measured versus predicted peak concentrations for Thorney Island TrialNo. 13 via using various K-models.

wind horseshoe shape is probably a result of the wake effects. The vertical profile shown in Fig. 9(b), namely,a thin upwind edge and a thick nose-shaped downwind front, is the combined result of a strong shear, high turbulent diffusion in the ambient wind and a weak negative buoyancy force in the cloud. Such a cloud profile closely resembles what has been observed in the laboratory and field (see, Fig. 13 of Hall and Waters [29]).

In Fig. 10, the predicted peak concentrations along the downwind distance are compared with field measurements. Because Trial Nos. 13 and 18 have almost the same atmospheric conditions (7.5 m/s vs. 7.4 m/s in windspeed, and both of D stability) and comparable amount of source material (1950 m^3 at a density ratio of 2.00 vs. 1700 m^3 at a density ratio of 1.84), the measured data from both trials are included here for comparisons. Although the two trials have similar release and atmospheric conditions, the measured peak values of concentration differ considerably. Such variability in field experiments should be taken into consideration in model–data comparisons. Compared with the data of Trial No. 13, FEM3 predictions are too low; however, the model results agree much better with the data from Trial No. 18. Again, the discrepancy between FEM3 predictions and field data can be attributed to those factors discussed in Trial No. 9, namely, the inappropriateness of the turbulence submodel used for the early phases of release, the variability in field experiments, and the uncertainty about the averaging time to be used for model–data comparisons.

To demonstrate the effects of "turbulence modeling", results from three variants of the K-model used in FEM3 are compared in Fig. 11. The three models

are: the previous K-model (Ri defined by eqn. (8) and $\alpha = 0.05$), the ambient K-model ($Ri = Ri_a = z/L$), and the present K-model (Ri defined by eqn. (8) with the second term on the right hand side replaced by eqn. (11)). It is seen that, without the density stratification term to damp out the turbulence in the cloud, the ambient K-model underpredicted the peak concentrations by a factor of nearly 2 for the entire curve. The previous K-model improved the agreement considerably near the source ($x < 100$ m), beyond which the agreement is poorer. The present K-model has obviously yielded the best agreement but, as stated earlier, further improvement is necessary to better simulate the early phases of the release.

3.4 Trial No. 17

In Trial No. 17, pure Freon-12 gas, 1,700 m^3 of 4.2 relative density, was released under a moderate wind speed of 5 m/s and slightly stable atmospheric conditions. The graded mesh used in Trial No. 13 was also used in this simulation. The ambient velocity profile on the upwind boundary was specified to be

$$u = 3.25 + 0.204z - 0.003z^2 \qquad m/s.$$

Although in every aspect of the release and atmospheric conditions except the initial relative density, Trial No. 17 is closer to Trial No. 13 than Trial No. 9 (see Table 1), the resulting gas cloud turned out to be more similar to that of Trial No. 9. It is believed the explanation is related to the very high values of initial Richardson number in Trials 9 and 17. Depicted in Fig. 12 are the predicted concentration contours for the 0.4 m horizontal plane and the vertical symmetry plane at $t = 30$ s, when the maximum concentration has fallen to near 10%. Similar to Fig. 7 of Trial No. 9, this figure also shows a strong cloud bifurcation and a highly diluted source center. Due to its higher initial relative density, Trial No. 17 was observed to have a much higher velocity (~ 16 m/s at $t = 6$ s) during the gravity slumping phase, thus producing a larger highly-diluted source region as shown in the figure. Like Trial No. 9, at the time of comparable maximum concentration, gravity spreading is still present to cause the cloud to expand horizontally. The predicted maximum extent of the 1% contour reached about 40 m upwind and 160 m in the crosswind direction.

In Fig. 13, the predicted concentrations for two crosswind planes behind the source are shown for $t = 20$ and 30 s, respectively, when the selected concentration contours reached their respective highest positions. Due to the presence of very high frequency components in most of the time series of concentration data and insufficient number of concentration measurements in the selected crosswind planes, it is difficult to construct the corresponding contours for the experiment. Instead, the observed peak values (over all times) for sensors near the selected crosswind planes and at heights of 2.4, 4.4, and 6.4 m, respectively,

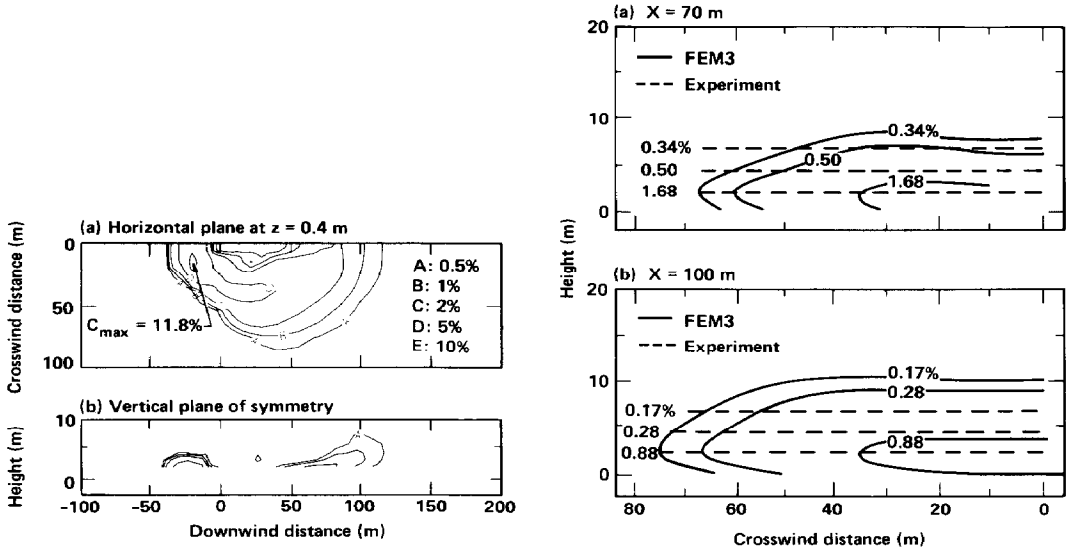

Fig. 12. Predicted concentration contours for Thorney Island Trial No. 17 at $t = 30$ s.

Fig. 13. Comparison of maximum heights for selected concentration levels on two crosswind planes of Thorney Island Trial No. 17.

are used here for comparisons. Also, because it is generally difficult to determine the exact lateral locations of the peak values due to the possible effects of cloud meandering, the experimental peak values are presented as horizontal dashed lines rather than fixed points. From this figure, a qualitative comparison of the predicted versus observed cloud height can be made. In general, the agreement between model predictions and measurements is fairly good, although the predicted cloud is higher. In Fig. 13(b), the 0.88% contour has "lifted" off the ground (as also indicated in Fig. 12(b)), which is believed to be due to the large shear existing in the ambient flow as well as the radial momentum acquired by the slumping phase. A similar vertical concentration profile was observed in the field experiment (see Fig. 16.9 of McQuaid and Roebuck [30]). In this trial, an 8-sensor mast was deployed at 75 m from the release point and the measured peak concentrations showed a second concentration maximum at 3.5 m, in addition to the one normally expected near the ground (not measured in the field test).

In Fig. 14, the predicted peak values of concentration at 0.4 m height are compared with field measurements. Although the curve predicted by FEM3 is still somewhat below the measured data, the agreement in this case is considerably better than the two previous cases. The poor agreement in the far field may be a result of uncertainty on the experimental peak value at 500 m. A close examination of the concentration records at this location reveals some spikes,

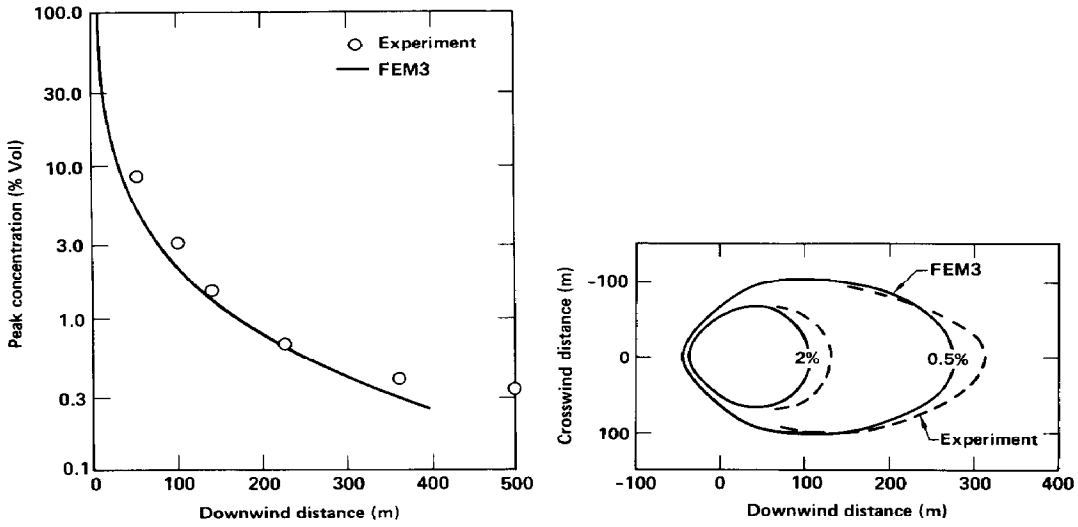

Fig. 14. Predicted versus measured peak concentrations for Thorney Island Trial No. 17 (at height = 0.4 m).

Fig. 15. Predicted versus measured peak concentration contours for Thorney Island Trial No. 17 (at height = 0.4 m).

which could be caused by the passage of small cloud puffs. A peak value of approximately 0.25%, instead of 0.35%, appears to be more realistic and should probably have been plotted for comparison.

In Fig. 15, a comparison is made for the peak concentration contours. The experimental curves were reconstructed from Fig. 8 of Davies and Singh [4] and the predicted curves were constructed from the maximum extent of the specified contours over all times. Although a slightly wider and shorter cloud was predicted by FEM3, the overall agreement between model predictions and data is good.

3.5 Other cloud characteristics

In Table 2, comparisons are made for various cloud characteristics, including cloud area increase rates, the maximum distances of the 1% concentration, and the times corresponding to the maximum downwind extent of the 1% concentration. The cloud area increase rates for the selected experiments were obtained by Brighton et al. [31], based on overhead photographs. Because there is uncertainty about the concentration level corresponding to the edge of the cloud as seen in the overhead photographs, two sets of numbers (based on the 0.1% and 0.5% concentration contours) were given from the model predictions. The model results were obtained by first calculating the areas enclosed by the respective contour level for the 0.4 m horizontal plane, and then plotting

TABLE 2

Predicted and observed cloud characteristics

Trial Number	9		13		17	
	Predicted	Observed	Predicted	Observed	Predicted	Observed
Cloud area increase rate, (m^2/s)						
0.1% contour	480		920		720	
Overhead photographs		480		517§		617§
0.5% contour	400		445		490	
Distances to 1% conc. (m)						
Upwind	70	>70	20	N/A	40	N/A
Crosswind	220	265	130	150*	160	155
Downwind	215	320	270	355	170	190
Times to 1% conc. (s)						
Downwind	300	450	110	100	110	140

*Due to the sparseness of data in the crosswind direction, this value is highly interpretative.
§Significant portion of cloud was not visible against the runway [31].

the areas versus time. All the curves so constructed were observed to vary almost linearly in time, up to at least $t=50$ s. For simplicity, the average area increase rates for times 0 and 50 s were adopted here. For Trial No. 9, the two numerical values are fairly close, indicating the existence of a well-defined cloud boundary. However, for Trial No. 13, due to high windspeed and less stable atmospheric conditions, more intensive turbulent mixing occurred on the cloud boundary, thus yielding a less distinct cloud/air interface. The area increase rates given by the two contours differ slightly more than a factor of 2. For Trial No. 17, the variation between the two numerical values is in between. Except for the value corresponding to the 0.1% concentration in Trial No. 13, the discrepancies between model predictions and data are about 20%.

Also compared in the table are the maximum distances of the 1% concentration in the upwind, crosswind, and downwind directions. The experimental values were obtained from the peak values of the time series of concentration, along with linear interpolation between sensors, where necessary. The FEM3 model is seen to under-predict the downwind distance in all cases, as observed previously. The predicted distances in the crosswind direction, however, are generally better. Overall, the agreement between model predictions and data is good. Regarding the times corresponding to the maximum downwind distances of the 1% concentration, the agreement is very good for Trials Nos. 13 and 17; for Trial No. 9, the numerical model appears to predict a cloud too quickly diluted to below 1%.

3.6 Computational costs

All the simulations reported herein were performed on a one-million word CRAY-1 computer. For each trial, a steady-state flow field around the source structure was calculated first, which was then followed by simulation of the instantaneous gas release and dispersion. The pressure field in all cases was solved via an ICCG method [32] with all matrices contained in memory to minimize I/O cost. Summarized below are the storage requirements and computing costs pertaining to the gas dispersion simulation for each of the trials (the cost for obtaining the steady state flow field was only a small fraction compared to the total cost for each simulated trial). Trial No. 9 had slightly over 51,000 algebraic equations and required approximately 700K decimal words in memory. The dispersion simulation for seven minutes was performed in 15,900 time steps and took approximately 3.5 h computer time. The problem sizes of Trial Nos. 13 and 17 are the same, each with approximately 30,000 algebraic equations and requiring 430K memory spaces. The gas dispersion of Trial No. 13 was simulated for 2 min with 2,700 time steps and took 0.4 h, while Trial No. 17 was simulated for 4 min with 18,250 time steps and took slightly over 2 h computer time.

4. Concluding remarks

In this paper, the FEM3 model has been applied to simulate three of the Thorney Island Phase I trials, namely, Nos. 9, 13, and 17. These selected trials represent releases ranging from low wind speed and stable atmospheric conditions to strong wind and neutral stability, with initial relative density varying from 1.6 to 4.2. The concentration data collected on a 100 m grid spacing were found to provide adequate resolution for determining the downwind distances of selected concentration levels. The crosswind distances, however, had to be obtained by using a linear interpolation scheme of the concentrations to provide suitable data for a meaningful model–data comparison.

Based on the results of this study, the model predictions of peak concentrations are consistently below field data by as much as a factor of 2 in one of the cases. Although the uncertainties regarding the appropriate averaging time and the variability in field experiments may contribute to some of the discrepancies, the adequacy of the present turbulence submodel during the early phases of the releases is also questionable. The present model, which is basically a local equilibrium model based on the similarity functions established in steady atmospheric boundary layers, is not intended for the early phases of an instantaneous release, which generally involve highly transient and very complex flow phenomena. To model such complex flow and dispersion scenarios accurately, a more sophisticated turbulence submodel would be necessary.

Despite some underpredictions, the calculated peak concentration curves are consistent with field measurements regarding their shapes and relative

positions. Also, the FEM3 model appears to predict well most of the salient features present in a large, instantaneous heavy gas release, specifically the gravity slumping and spreading, formation of the doughnut-shaped cloud with a highly-diluted source center, and cloud bifurcation. The predicted major cloud characteristics, including cloud area increase rates, critical distances and cloud arrival times, also agree well with field measurements.

Recently the meteorological data have been further analyzed by Puttock [33] and some differences with the data used herein (which have been inferred from [3] and [22]) were reported. Apparently these differences would have some impact on the quantitative results reported herein. However, because the changes are not significant relative to the dominance of gravity spreading in all the trials, the basic conclusions are expected to remain the same.

There has been a lot of attention given to area-averaged concentrations, such as those predicted by box models (see, for example, Brighton [34]). Although box models are not considered to be appropriate for the early (initial slumping and gravity-spreading) phases of an instantaneous release, they are appropriate and very efficient in modeling the subsesquent phases of gas dispersion, after the cloud becomes well-mixed and near uniform. Under such conditions, direct comparisons between the cloud average properties from a three-dimensional model (such as FEM3) and the results of box models would be meaningful and, through such comparisons, more effective use of three-dimensional and box models could probably be established.

Since FEM3 can deal with gas dispersion over complex terrain and in the presence of obstacles, a further test and validation of the model would be comparisons with the Thorney Island Phase II trials and the pending LNG vapor fence experiments sponsored by the U.S. Department of Transportation and the Gas Research Institute. In such cases, however, meshes finer than those used for gas dispersion without obstructions will inevitably be required and a more sophisticated turbulence submodel would be necessary in order to model the complex dispersion scenarios accurately.

Acknowledgements

This Work was performed under the auspices of the U.S. Department of Energy by the Lawrence Livermore National Laboratory under Contract No. W-7405-ENG-48.

References

1 S.T. Chan, FEM3 - A finite element model for the simulation of heavy gas dispersion and incompressible flow: User's manual, UCRL-53397, Lawrence Livermore National Laboratory, Livermore, CA. 1983.

2 P.M. Gresho, S.T. Chan, C.D. Upson and R.L. Lee, A modified finite element method for solving the time-dependent, incompressible Navier-Stokes equations: Part 1, Theory; Part 2, Applications, Int. J. Num. Meth. Fluids, 4 (1984) 557-598, 619-640.

3 J. McQuaid, Objectives and design of the Phase I heavy gas dispersion trials, J. Hazardous Materials, 11 (1985) 1-33.

4 M.E. Davies and S.Singh, The Phase II trials: A data set on the effect of obstructions, J. Hazardous Materials, 11 (1985) 301-323.

5 R.P. Koopman, R.T. Cederwall, D.L. Ermak, H.C. Goldwire, Jr., W.J. Hogan, J.W. McClure, T.G. McRae, D.L. Morgan, H.C. Rodean and J.H. Shinn, Analysis of Burro series 40-m^3 LNG spill experiments, J. Hazardous Materials, 6 (1982) 43-83.

6 D.L. Ermak, S.T. Chan, D.L. Morgan and L.K. Morris, A comparison of dense-gas dispersion model simulations with Burro series LNG spill test results, J. Hazardous Materials, 6 (1982) 129-160.

7 S.T. Chan, H.C. Rodean and D.L. Ermak, Numerical simulations of atmospheric releases of heavy gases over variable terrain, In: C. De Wispelaere (Ed.), Air Pollution Modeling and its Application, Part III, Plenum Press, New York, 1984, pp. 295-341.

8 H.C. Goldwire, Jr., H.C. Rodean, R.T. Cederwall, E.J. Kansa, R.P. Koopman, J.W. McClure, T.G. McRae, L.K. Morris, L.M. Kamppinen, R.D. Kiefer, P.A. Urtiew and C.D. Lind, Coyote Series Data Report, LLNL/NWC 1981 LNG spill tests, dispersion, vapor burn, and rapid phase transitions, UCID-19953, Vols. 1 and 2, Lawrence Livermore National Laboratory, Livermore, CA, 1983.

9 D.L. Morgan, Jr., L.K. Morris, S.T. Chan, D.L. Ermak, T.G. McRae, R.T. Cederwall, R.P. Koopman, H.C. Goldwire, Jr., J.W. McClure and W.J. Hogan, Phenomenology and modeling of liquefied natural gas vapor disersion, UCRL-53581, Lawrence Livermore National Laboratory, Livermore, CA, 1984.

10 D.L. Ermak and S.T. Chan, A study of heavy gas effects on the atmospheric dispersion of dense gases. In: C. De Wispelaere et al. (Ed.), Air Pollution Modeling and its Application, Part V, Plenum Press, New York, 1986, pp. 723-742.

11 T.G. McRae, Analysis and model/data comparisons of large-scale releases of nitrogen tetroxide, UCID-20388, Lawrence Livermore National Laboratory, Livermore, CA, 1985.

12 S.T. Chan and D.L. Ermak, Further assessment of FEM3 - A numerical model for the dispersion of heavy gases over complex terrain, UCRL-92497, Lawrence Livermore National Laboratory, Livermore, CA, presented at the 1985 JANNAF S&EP Subcommittee Meeting, Monterey, CA, November 4-8, 1985.

13 G.W. Colenbrander, A.E. Evans and J.S. Puttock, Spill tests of LNG and refrigerated liquid propane on the sea, Maplin Sands, 1980: Dispersion data digists, Shell Thornton Research Center, 1984.

14 D.L.Ermak and S.T. Chan, Recent developments on the FEM3 and SLAB atmospheric dispersion models, UCRL-94071, Lawrence Livermore National Laboratory, Livermore, CA. To appear in the proceedings of the IMA Conference on Stably Stratified Flows and Dense-Gas Dispersion, Chester, England, April 9-10, 1986.

15 J. McQuaid, Some experiments on the structure of stably stratified shear flows, Technical Paper P21, Safety in Mines Research Establishment, Sheffield, U.K., 1976.

16 E.J. Kansa, D.L. Ermak, S.T. Chan and H.C. Rodean, Atmospheric dispersion of ammonia: an ammonia fog model, UCRL-88649, Lawrence Livermore National Laboratory, Livermore, CA, 1983.

17 J.M. Leone, Jr., H.C. Rodean and S.T. Chan, FEM3 phase change model, UCID-20353, Lawrence Livermore National Laboratory, Livermore, CA, 1985.

18 P.H. Gudiksen, M.H. Dickerson, S.T. Chan, L.K. Morris, D.L. Ermak, M. Brown, J. Perry, M. Vonada and L. Robinson, Emergency response planning for potential accidental liquid chlorine releases, UCRL-53685, Lawrence Livermore National Laboratory, Livermore, CA, 1986.

19 Y. Ogura and N. Phillips, Scale analysis of deep and shallow convection in the atmosphere, J. Atmos. Sci., 19 (1962) 173–179.
20 R.L. Lee, P.M. Gresho, S.T. Chan and C.D.Upson, A three-dimensional, finite element model for simulating heavier-than-air gaseous releases over variable terrain, In: C. De Wispelaere (Ed.), Air Pollution Modeling and Its Applications, Part II, Plenum Press, New York, 1983, pp. 555–573.
21 A.J. Dyer, A review of flux-profile relationships, Boundary-Layer Meteorol., 7 (1974) 363–372.
22 M.E. Davies and S. Singh, Thorney Island: Its geography and meteorology, J. Hazardous Materials, 11 (1985) 91–124.
23 Health and Safety Executive, Heavy Gas Dispersion Trials, Thorney Island, 1982–83, Research and Laboratory Services Division, Health and Safety Executive, Sheffield, U.K., 1983.
24 J.W. Rottman, J.C.R. Hunt and A. Mercer, The initial and gravity-spreading phases of heavy gas dispersion: Comparison of models with Phase I data, J. Hazardous Materials, 11 (1985) 261–279.
25 P.M. Gresho and R.L. Lee, Don't suppress the wiggles – They're telling you something, Comput. Fluids, 9 (2) (1980) 223–255.
26 T.O. Spicer and J.A. Havens, Modeling the Phase I Thorney Island experiments, J. Hazardous Materials, 11 (1985) 237–260.
27 J.S. Puttock and G.W. Colenbrander, Thorney Island data and dispersion modelling, J. Hazardous Materials, 11 (1985) 381–397.
28 C. Nussey, J.K.W. Davies and A. Mercer, The effect of averaging time on the statistical properties of sensor records, J. Hazardous Materials, 11 (1985) 125–153.
29 D.J. Hall and R.A. Waters, Wind tunnel model comparisons with the Thorney Island dense gas release field trials, J. Hazardous Materials, 11 (1985) 209–235.
30 J. McQuaid and B. Roebuck, Large-scale field trials on dense vapour dispersion, Research and Laboratory Services Division, Health and Safety Executive, Sheffield, U.K.
31 P.W.M. Brighton, A.J. Prince and D.M. Webber, Determination of cloud area and path from visual and concentration records, J. Hazardous Materials, 11 (1985) 155–178.
32 D. Kershaw, The incomplete Cholesky-conjugate gradient method for the iterative solution of systems of linear equations, J. Comp. Phys., 26 (1978) 43–65.
33 J.S. Puttock, Analysis of meteorological data for the Thorney Island Phase I trials, Second Symposium on Heavy Gas Dispersion Trials at Thorney Island, Sheffield, U.K., September 1986, J. Hazardous Materials, 16 (1987) 43–74.
34 P.W.M. Brighton, Area-averaged concentrations, height-scales and mass balances, J. Hazardous Materials, 11 (1985) 189–208.